ORIGINAL RESEARCH

Effect of La³⁺ substitution on structural and magnetic parameters of Ni–Cu–Zn nano-ferrites

B. B. Patil[1] · A. D. Pawar[1] · D. B. Bhosale[1] · J. S. Ghodake[2] · J. B. Thorat[3] · T. J. Shinde[1]

Abstract

The ferrite material with compositions $Ni_{0.7}Cu_{0.1}Zn_{0.2}La_xFe_{2-x}O_4$ (where $x = 0$, 0.015, 0.025, and 0.035) was synthesized by oxalate co-precipitation method. The ferrite samples were characterized by thermo-gravimetric and differential temperature analysis (TG–DTA), energy-dispersive X-ray analysis (EDAX), X-ray diffraction (XRD), Fourier transform infrared spectroscopy (FTIR), field-emission scanning electron microscopy (FE-SEM), and vibrating sample magnetometer (VSM) techniques. The EDAX analysis confirmed the formation of required stoichiometric ferrite samples. The formation of cubic spinel structure with the presence of weak ortho-ferrite phases was confirmed from X-ray diffraction analysis. The lattice constant of all the ferrites was found to be increase with increase in La³⁺ content. The presence of main two recognized strong absorption bands in the frequency range 400–600 cm⁻¹ in the FTIR spectra shows the formation of well spinel ferrite. Morphological study shows that grain size of the ferrites lies in the range 16.23–24.21 nm. It is observed that the saturation magnetization and magnetic moment of Ni–Cu–Zn ferrites decrease with La³⁺ content.

Keywords Ni–Cu–Zn nano-ferrite · XRD · FTIR · FE-SEM · VSM

Introduction

Soft-ferrite materials are mostly useful material because of its technological and industrial applications. These applications are depending on their properties such as high resistivity, moderate permeability, low dielectric loss, low permittivity, etc. These properties play an important role in the fabrication of components such as a transformer core, antenna rods, multi-layer chip inductor, micro-inductors, electromagnetic filters, etc. [1–4]

Recently, researchers synthesized ferrites in the form of nanoscale range because of its growing applications such as production of bio-diesel [5], nano-catalyst [6], humidity sensor [7], gas sensor [8], super-capacitor [9], electrode material for Li-ion battery [10], etc. Various methods such as sol–gel auto-combustion, co-precipitation, citrate precursor, wet chemical route, hydrothermal [11–15], etc. were used for the preparation of nano-ferrite materials.

In the last decade, researchers investigated various properties of Ni–Zn ferrites due to their interesting properties such as high resistivity, high permeability, and low eddy current losses. Recently, Ni–Zn ferrite material was used in high-frequency applications such as multi-layer chip inductors and electromagnetic interference filters. Das and Singh [16] investigated the structural, magnetic, and dielectric properties of Cu-substituted Ni–Zn ferrites. They reported that the coercivity and saturation magnetization of Ni–Zn ferrites improved by substituting Cu content. Avati et al. [17] illustrated that the poor

✉ B. B. Patil
  bajrangpatil44@gmail.com

  A. D. Pawar
  pawaramold89@gmail.com

  D. B. Bhosale
  dheerajtvishaa@gmail.com

  J. S. Ghodake
  jeevan.ghodake@rediffmail.com

  J. B. Thorat
  jayavantt@rediffmail.com

  T. J. Shinde
  pshindetj@yahoo.co.in

1 P. G. Department of Physics, Smt. KRP Kanya
   Mahavidyalaya, Islampur, Maharashtra 415409, India

2 Department of Physics, PDVP Mahavidyalaya, Tasgaon,
   Maharashtra 416 312, India

3 Department of Physics, Arts, Science and Commerce
   College, Ramanandnagar, Maharashtra 416308, India

densification and slow grain growth rate of Ni–Zn ferrites can be greatly improved by the substitution of Cu^{2+} ions. In last few years, physicists synthesized Ni–Cu–Zn ferrites for the fabrication of electronic devices instead of Ni–Zn and Mg–Zn ferrites. Recently, it was found that properties of Ni–Cu–Zn nano-ferrites are extremely improved due to incorporation of rare earth metals. Shirsath et al. [18] investigated magnetic properties of Dy^{3+}-substituted Ni–Cu–Zn ferrite nanoparticles. They reported that the saturation magnetization, initial permeability, and Curie temperature of the ferrites enhance by Dy^{3+} substitution. Chaudhari et al. [19] investigated the crystallographic, magnetic, and electrical properties of $Ni_{0.5}Cu_{0.25}Zn_{0.25}La_xFe_{2-x}O_4$ nano-ferrites. They found that the lattice constant, porosity, and specific surface area were increased, whereas particle size, bulk density, saturation magnetization, and coercively of Ni–Cu–Zn ferrites were decreases with increasing La^{3+} content. On La^{3+} substitution, the structural parameters such as relative density, grain size, crystallite size, and density increase, and on the other hand, porosity, anisotropy, and compressive macro-stress of Ni–Cu–Zn ferrites decrease [20]. Roy [21] et al. studied electromagnetic properties of La-substituted Ni–Cu–Zn ferrites. They reported that the initial permeability and saturation magnetization of Ni–Cu–Zn ferrites increase on substitution of small fraction of La^{3+} ions. Gabal et al. [22] synthesized La-substituted Ni–Cu–Zn ferrites by sol–gel technique. They were studied its structural and magnetic properties and reported that the saturation magnetization and Curie temperature of ferrites decrease with increase in La^{3+} content. They attribute it to the decreasing of Fe^{3+}–Fe^{3+} interactions on the octahedral (B) sites. Structure and magnetic properties of Ni–Cu–Zn ferrite materials with La doping were investigated by Yuan-Xun et al. [23]. They showed that with La^{3+} substitution, saturation magnetization and complex permeability of Ni–Cu–Zn ferrites increase. Most of the researches [19, 23] have been prepared La^{3+}-substituted Ni–Cu–Zn ferrites by sol–gel method and ceramic method.

On literature survey, it was found that there is no any work carried out on La^{3+}-substituted Ni–Cu–Zn ferrites prepared by oxalate co-precipitation method at lower sintering temperature. The oxalate co-precipitation technique is important and attractive technique used for the preparation of nano-sized ferrite materials because of its advantages such as good stoichiometric control, the production of ultrafine particles with low sintering temperature, and smaller duration as compared to ceramic method.

The purpose of this work is to synthesize La^{3+}-substituted Ni–Cu–Zn nano-ferrites at lower sintering temperature followed by oxalate co-precipitation method and study its structural and magnetic properties.

Experimental

Synthesis of La^{3+}-substituted Ni–Cu–Zn ferrites

Lanthanum-substituted Ni–Cu–Zn nano-ferrites with chemical formula $Ni_{0.7}Cu_{0.1}Zn_{0.2}La_xFe_{2-x}O_4$ (where $x = 0$, 0.015, 0.025, and 0.035) were prepared by oxalate co-precipitation method. The AR grade nickel sulphate ($NiSO_4\ 6H_2O$), copper sulphate ($CuSO_4\ 5H_2O$), zinc sulphate ($ZnSO_4\ 7H_2O$), iron sulphate ($FeSO_4\ 7H_2O$), and lanthanum sulphate octahydrate [$La_2(SO_4)_3\ 8H_2O$] were used as a starting materials supplied by Thomas Becker.

The required stoichiometric sulphates were dissolved in the double-distilled water. The pH of the solution was maintained at 4 by adding dropwise conc. H_2SO_4 and heated for 2 h for proper mixing of all the sulphate. After cooling, super-saturated solution of ammonium oxalate was added in the solution until to complete the process of precipitation. A solution with precipitation placed on the sand bath for shrinkage. Due to this, the precipitates settle down at the bottom of beaker. The precipitate was filtered by Whatman filter paper no 41 using Buckner funnel and vacuum pump. The precipitate was washed several times to remove sulphate ions. The removal of sulphate ions in the precipitate was confirmed by barium chloride test and dried under radiation of IR light to remove water content. Pre-sintering and sintering temperatures in the investigation were decided by analyzing the precipitated powder by thermo-gravimetric and differential temperature analysis (TG–DTA). The resulting oxalate powder was pre-sintered at 300 °C for 2 h. After cooling, the pre-sintered powder was milled in agate mortal with acetone base. The powder was then sintered at 600 °C for 4 h. The sintered powder was again milled to have a fine powder. Pre-sintering and sintering process were carried out in the muffle furnace. Heating and cooling rate of the furnace were maintained at 80 °C/h.

The process of synthesis of La^{3+}-substituted $Ni_{0.7}Cu_{0.1}Zn_{0.2}La_xFe_{2-x}O_4$ (where $x = 0$, 0.015, 0.025, and 0.035) by oxalate co-precipitation method is shown diagrammatically in Fig. 1.

Characterization

The thermo-gravimetric (TG) and differential thermal analysis (DTA) of prepared oxalate nano-powder was carried out by SDT Q600 V20.9 build 20 instrument in air atmosphere with heating rate of 10 °C/min in the range 25–1000 °C by ramp method. The crystal structure, phase purity, crystallite size, and other parameters were studied by X-ray powder diffractometer (Phillips, Model 3710) with Cu-Kα radiation ($\lambda = 1.5425$ Å). The elemental composition of prepared ferrite was tested by Energy-Dispersive X-ray

spectroscopy (EDAX) model ASTM E1508-98 Oxford. The Fourier transform infrared spectroscopy (FTIR) analysis was carried out in the range 350–800 cm^{-1} by compositing the ferrite powder into KBr discs by Bruker ALPHA 100508 at room temperature. The morphology and grain size of nano-ferrite powder were studied with Zeiss Ultra 55 field effect-scanning electron microscopy (FE-SEM). The magnetic parameters such as saturation magnetization, remanence magnetization, coercivity, magnetic moment, and anisotropy constant of all the ferrites were obtained from vibrating sample magnetometer (PFM-Magneto make model) at room temperature.

Results and discussion

### Thermo-gravimetric and differential temperature analysis

A typical TG–DTA curve for the oxalate powder prepared for $Ni_{0.7}Cu_{0.1}Zn_{0.2}La_{0.035}Fe_{1.965}O_4$ is shown in Fig. 2. The TGA curve exhibits two distinct weight loss steps corresponding to endothermic peak and exothermic peaks of DTA curve.

The TGA curve initially shows 19.95% weight loss in the range 116.13–212.98 °C. During this loss, endothermic peak exhibits at 204.91 °C in DTA curve and represents the evaporation of water and other elements is completed.

Further TGA curve shows 36.15% weight loss in the range 212.98–366.33 °C with existence of an exothermic peak at 298.73 °C of DTA curve. This shows that decomposition of oxalate was completed at 366.33 °C and confirms the formation of phase in the material. Above 366.33 °C, TGA plot shows no further weight loss.

Murbe and Topfer [24] synthesized Ni–Cu–Zn ferrites by oxalate precursor method using Ni, Cu, and Zn acetate hydrate as starting materials. They observed quite similar behavior for TG–DTA plot. They found that thermal decomposition of the oxalate hydrate was completed at 300 °C. DTA and TG analysis of Ni–Cu–Zn ferrites prepared by sol–gel auto-combustion method was reported by Yue et al. [25]. They observed exothermic peak at about 220 °C and attributed to the reaction of nitrates with citric acid, whereas the exothermic peak at about 400 °C corresponds to the decomposition of citric acid. Wei-chi-Hsu et al. [26], Ramakrishna et al. [27], Shifeng-yan et al. [28], and Humbe et al. [29] also studied the thermo-gravimetric and differential temperature analysis for Ni–Cu–Zn ferrites.

Fig. 1 Diagrammatic synthesis procedure of La^{3+} substituted Ni–Cu–Zn nano-ferrites by oxalate co-precipitation method
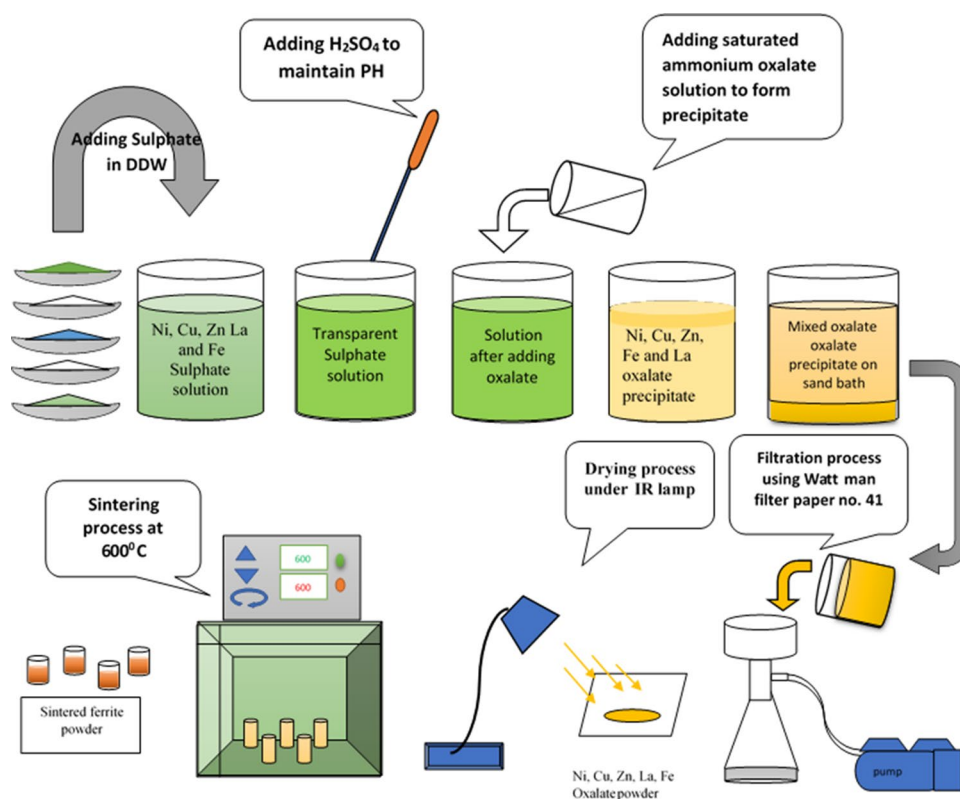
Energy-dispersive X-ray spectroscopy (EDAX) analysis

The EDAX of $Ni_{0.7}Cu_{0.1}Zn_{0.1}La_xFe_{2-x}O_4$ (where $x = 0.000$, 0.015, 0.025, and 0.035) system is shown in Fig. 3a–d. The presence of peaks corresponding to the elements Ni, Cu, Zn, La, Fe, and O in the spectra confirms the formation of appropriate respective ions in the material as per the initial stoichiometric considered without any other impurity ions. The compositional atomic percentage of Ni^{2+}, Cu^{2+}, Zn^{2+}, La^{3+}, Fe^{3+}, and O^{2-} ions in the all ferrites are tabulated in Table 1. From this table, it is found that the molar ratio of tetrahedral-to-octahedral site metal ions is approximately agree with theoretical ratio of respective ions and confirms the formation of required homogeneous stoichiometric ferrite under investigation.

XRD analysis of La^{3+}-substituted Ni–Cu–Zn ferrites

XRD patterns of $Ni_{0.7}Cu_{0.1}Zn_{0.2}La_xFe_{2-x}O_4$ (where $x = 0.000$, 0.015, 0.025, and 0.035) are shown in Fig. 4. The presence of (111), (220), (311), (222), (400), (422), (511), and (440) planes in the diffraction pattern confirmed the formation of cubic spinel structure [19, 20, 22] having Fd-3 m space group in addition with weak appearance of ortho-ferrite phase shown by the Star (*). The formation of ortho-ferrite phase is due to La–FeO_3. Chaudhary et al. [19] also observed ortho-ferrite phase for La^{3+}-substituted Ni–Cu–Zn ferrites synthesized by sol–gel method. From diffraction pattern, it is seen that the intensity of peaks decreases with increasing La^{3+} content up to $x = 0.025$ and thereafter increases for $x = 0.035$ (Table 2). It means that the lighter percentage of La^{3+} content diluted completely
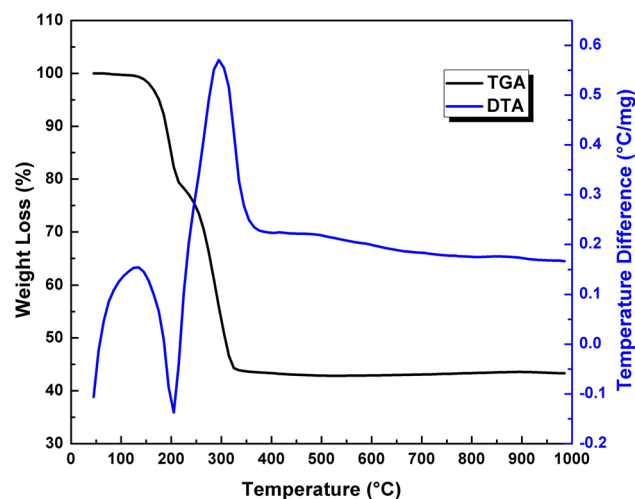
in ferrites having compositions $x \le 0.025$, but thereafter, there may be possibility of inappropriate dilution for the composition $x = 0.035$ content. The undiluted La^{3+} ions form the $LaFeO_3$ phase on the grain boundaries. Due to this, there may be insufficient diffraction centers in the nano-sized particles, which results increase in peak intensity for the composition $x = 0.035$ [30]. Chaudhary et al. [19] reported that the maximum limit for replacement of Fe^{3+} by La^{3+} in Ni–Cu–Zn ferrites is up to $x = 0.025$.

The lattice parameter 'a' of all the ferrites was calculated for most intense (311) peak using the formula:

$$a = d_{obs}\sqrt{h^2 + k^2 + l^2}, \tag{1}$$

where d_{obs} is the observed inter-planner spacing.

Lattice constant of all the ferrites is tabulated in Table 2. From this table, it is seen the lattice constant of Ni–Cu–Zn ferrites increases with increase in La^{3+} content. This is attributed to replacement of smaller ionic radii Fe^{3+} ions (0.67 Å) by larger ionic radii La^{3+} ions (1.05 Å). This indicates that La^{3+} ions occupy octahedral (B) site. Similar type of result was reported by Angari [31] and Gabal et al. [22] for La^{3+}-substituted Ni ferrites and Ni–Cu–Zn ferrites synthesized by egg-white precursor method. Roy et al. [20] synthesized La^{3+} substituted Ni–Cu–Zn ferrites by citrate nitrate auto-combustion method. They found that there is no any remarkable trend for lattice constant of La^{3+}-substituted Ni–Cu–Zn ferrites.

The X-ray density (ρ_x) of all the ferrites was calculated using the formula [32]:

$$\rho_x = \frac{8M}{Na^3}, \tag{2}$$

where M is the molecular weight, N is an Avogadro's number.

It is seen that the X-ray density of La^{3+}-substituted ferrites are higher than pure Ni–Cu–Zn ferrite, but shows fluctuation trend with La^{3+} content. In our investigation, it is observed that M as well as lattice constant (a) increases with increasing La^{3+} content. Thereby, the ratio (M/a^3) shows fluctuation trend with La^{3+} contents. That is why, X-ray density shows fluctuation trend with La^{3+} contents (Table 2).

The average crystallite size (D) of the ferrite powder was estimated for the most intense (311) peak of XRD using the Debye Scherer formula [32]:

$$D = \frac{0.9\lambda}{\beta\cos\theta}, \tag{3}$$

where λ is wavelength of used X-ray beam, β is the full-width at half-maxima, θ is diffracting angle.

Obtained crystallite size of the ferrites is presented in Table 2. From this table, it is seen that the crystallite size
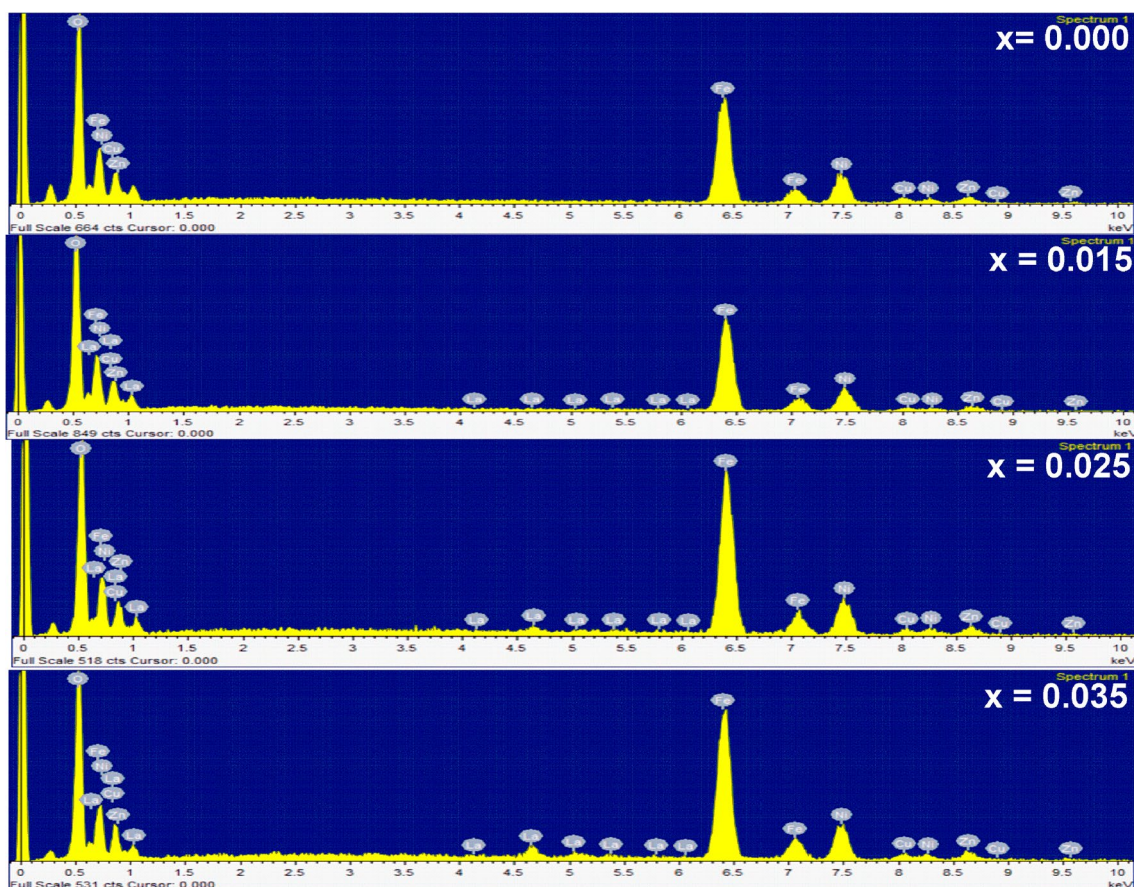

Fig. 2 TG-DTA plot for $Ni_{0.7}Cu_{0.1}Zn_{0.2}La_{0.035}Fe_{1.965}O_4$ system

Fig. 3 EDAX spectra for $Ni_{0.7}Cu_{0.1}Zn_{0.2}La_xFe_{2-x}O_4$ (where $x = 0.0$, 0.015, 0.025, and 0.035) system

Table 1 Atomic % of metal ions of $Ni_{0.7}Cu_{0.1}Zn_{0.2}La_xFe_{2-x}O_4$ (where $x = 0.000$, 0.015, 0.025, and 0.035) system

Content x	Atomic % of metal ions					
	Ni	Cu	Zn	La	Fe	O
0.00	9.16	1.90	2.59	–	22.19	64.16
0.015	7.57	1.15	2.19	0.03	21.50	67.56
0.025	9.18	1.55	2.91	0.50	27.86	58.01
0.035	9.50	1.40	2.99	0.94	26.71	58.46

of the ferrites decreases with increasing lanthanum content up to $x = 0.025$ and thereafter increases. It is known that the induced crystalline anisotropy increases with replacement of smaller ionic radii Fe^{3+} ions by larger ionic radii La^{3+} ions, which creates the strain inside the volume of the crystal [38]. This may result decrease in crystallites size with increase in La^{3+} contents except $x = 0.035$ composition. However, a crystallite size for the composition $x = 0.035$ is higher as compared to compositions $x = 0.015$ and 0.025. This may be due to inappropriate dilution of La^{3+} ions ($x = 0.035$) in Ni–Cu–Zn ferrite. Chaudhari et al. [19] also reported that the crystallite size of Ni–Cu–Zn ferrites decreases with increase in La^{3+} contents. The crystallite size for pure Ni–Cu–Zn

ferrite is higher than the La^{3+}-substituted Ni–Cu–Zn ferrite. Augustin et al. [33] reported the similar behavior for La^{3+} substituted strontium ferrite prepared by citrate combustion method.

Hopping lengths (L_A and L_B) are the distance between the magnetic ions in the respective sites. These lengths are calculated using the relations [19]:

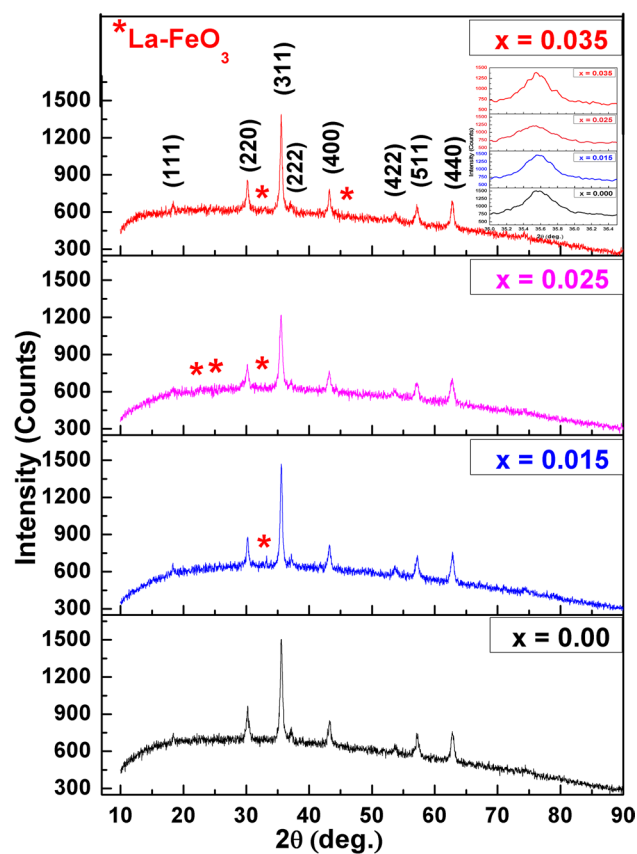$$L_A = a\sqrt{\frac{3}{4}} \tag{4}$$

$$L_B = a\sqrt{\frac{2}{4}}. \tag{5}$$

Fig. 4 X-ray diffraction patterns for $Ni_{0.7}Cu_{0.1}Zn_{0.2}La_xFe_{2-x}O_4$ (where $x = 0.0$, 0.015, 0.025, and 0.035) system

Bond lengths (A–O and B–O) and ionic radii (r_A and r_B) on A-site and B-sites were calculated using the relations suggested by Standley's:

$$A - O = \left(u - \frac{1}{4}\right)a\sqrt{3} \tag{6}$$

$$B - O = \left(\frac{5}{8} - u\right)a \tag{7}$$

$$r_A = \left(u - \frac{1}{4}\right)a\sqrt{3} - r_0 \tag{8}$$

$$r_B = \left(\frac{5}{8} - u\right)a - r_0. \tag{9}$$

The oxygen ionic radii $r_0 = 1.32$ Å [34] and oxygen ion parameter $u = 0.381$ are used for calculations. The hopping lengths, bond lengths, and ionic radii on A-site and B- site of all the ferrites are presented in Table 3. From this table, it is seen that the bond lengths, ionic radii, and hopping lengths on A-site as well as on B-sites are increased with incorporation of small amount of La^{3+} ions in pure Ni–Cu–Zn ferrites. This may be attributed to higher lattice constant for La^{3+}-substituted ferrites.

Fourier transform infrared spectroscopy

The position of absorption bands corresponding to tetrahedral (A), octahedral (B) sites, and the information about chemical changes in structure of ferrites is obtained from FTIR analysis. FTIR spectra of $Ni_{0.7}Cu_{0.1}Zn_{0.2}La_xFe_{2-x}O_4$ $(0.00 \leq x \leq 0.035)$ system recorded in the range 350–800 cm^{-1} are shown in Fig. 5. The higher frequency absorption band (v_1) corresponding to tetrahedral (A) site lies in the range 587–599 cm^{-1}, whereas lower frequency absorption band (v_2) corresponding to octahedral (B) site lies in the range 401–403 cm^{-1}. The change in the band position of v_1 arises due to the change in the bond length of Fe^{3+}-O^{2-} at octahedral site, whereas the change in band position of v_2 may be due to increasing concentration of Fe^{2+} ions during synthesis of ferrite material. The observed wave numbers v_1 and v_2 corresponding to tetrahedral and octahedral sites are presented in Table 3. From this table, it is seen that v_1 becomes higher and v_2 becomes lower than pure Ni–Cu–Zn ferrite. This trend observed in the wave numbers may be due to formation of Fe^{2+} ions during the synthesis process [19].

It is also observed that the absorption as well as broadening of bands for both tetrahedral and octahedral sites are greater for $x = 0.015$ composition as compared to other compositions. Absorption of v_1 and v_2 bands is very lower for $x = 0.025$ composition as compared to other compositions. In XRD analysis, we have reported similar type of interpretation for intensity.

Table 2 Crystallite size (D), lattice constant (a), X-ray density (ρ_x) grain size (G), and intensity (I) of $Ni_{0.7}Cu_{0.1}Zn_{0.2}La_xFe_{2-x}O_4$ (where $x = 0.000$, 0.015, 0.025, and 0.035) system

Composition	Crystallite size D (nm)	Lattice constant a (Å)	X-ray density ρ_X (gm/Cm^3)	Gain size G (nm)	Intensity I (A.U.)
$Ni_{0.7}Cu_{0.1}Zn_{0.2}Fe_2O_4$	25.98	8.3619	5.3659	24.21	1504.68
$Ni_{0.7}Cu_{0.1}Zn_{0.2}La_{0.015}Fe_{1.985}O_4$	20.14	8.3725	5.3729	23.40	1469.37
$Ni_{0.7}Cu_{0.1}Zn_{0.2}La_{0.025}Fe_{1.975}O_4$	15.93	8.3843	5.3690	17.69	1218.74
$Ni_{0.7}Cu_{0.1}Zn_{0.2}La_{0.035}Fe_{1.965}O_4$	23.77	8.3936	5.3698	16.23	1387.34

Table 3 Ionic radii, bond lengths, hopping lengths, wave numbers, and force constants of $Ni_{0.7}Cu_{0.1}Zn_{0.2}La_xFe_{2-x}O_4$ (where $x=0.000$, 0.015, 0.025, and 0.035) system

La^{3+} content x	Ionic radii (Å)		Bond length (Å)		Hopping length (Å)		Wave numbers (cm^{-1})		Force constant (dyne/cm)	
	r_A A-site	r_B B-site	A–O A-site	B–O B-site	L_A A-site	L_B B-site	ϑ_1 A-site	ϑ_2 B-site	K_t A-site	K_o B-site
0.000	0.5787	0.7195	1.8987	2.0395	7.2416	5.9128	587.36	403.81	268663	100487
0.015	0.5811	0.7221	1.9011	2.0421	7.2508	5.9202	599.60	401.77	280652	99476
0.025	0.5838	0.7249	1.9038	2.0445	7.2610	5.9286	595.52	401.77	277142	99476
0.035	0.5859	0.7272	1.9059	2.0472	7.2691	5.9352	595.52	401.77	277455	99476
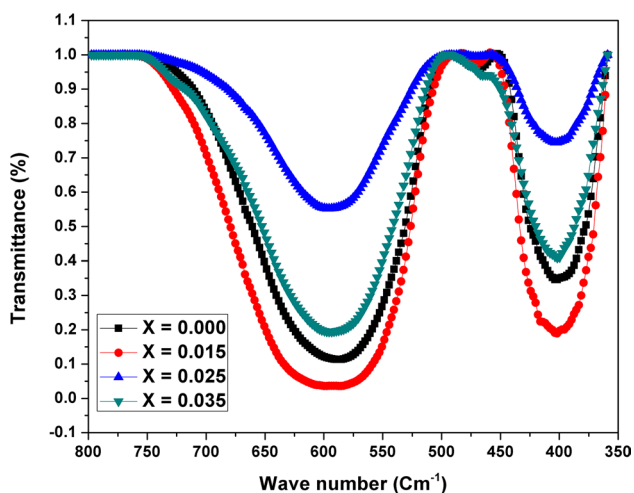
Fig. 5 FTIR spectra for $Ni_{0.7}Cu_{0.1}Zn_{0.1}La_xFe_{2-x}O_4$ (where $x=0.0$, 0.015, 0.025, and 0.035) system

The force constant on tetrahedral site (K_t) and on octahedral site (K_0) was calculated using the relations suggested by Waldron's [35]. The values of K_t and K_0 of all the ferrites are presented in Table 3. From this table, it is observed that K_t is lies in the range 2.686×10^5 to 2.806×10^5 dyne/cm and K_o lies in the range 0.9994×10^5 to 1.0048×10^5 dyne/cm. It is clear that K_t is greater than K_0. Kabbur et al. [34] evaluated values of K_t and K_o for Dy^{3+}-substituted Ni–Cu–Zn ferrites prepared by sol–gel auto-combustion method. They also observed that K_t is greater than K_o for all the compositions. It is also seen that the trends of K_t and K_0 of ferrites are similar to that observed for v_1 and v_2.

Field-emission scanning electron microscopy

FE-SEM micro-photographs of $Ni_{0.7}Cu_{0.1}Zn_{0.2}La_xFe_{2-x}O_4$ (where $x=0.0$, 0.015, 0.025, and 0.035) system are presented in Fig. 6. From these micrographs, it is clear that the formation of ferrite particles is approximately spherical. The grain size of the ferrite was calculated using linear intercept method [32] and its values are presented in Table 2. It is

seen that the grain size of the Ni–Cu–Zn ferrites decreases with increase in La^{3+} content. Similar type of result was reported by Chaudhary et al. [19] and Ikram et al. [36] for La^{3+}-substituted Ni–Cu–Zn ferrite and La^{3+}-substituted Ni–Cd–Zn ferrite nanoparticles prepared by sol–gel method.

VSM analysis

Figure 7 shows the hysteresis loops of $Ni_{0.7}Cu_{0.1}Zn_{0.2}La_xFe_{2-x}O_4$ (where $x=0.000$, 0.015, 0.025, and 0.035) system. The magnetic parameters such as saturation magnetization (M_S), retentively (M_r), and coercivity (H_C) obtained from the loops are listed in Table 4. These parameters are depending on the chemical composition, grain size, porosity, density, method of preparation, sintering process, and heat treatment conditions of ferrites [34]. From Table 4, it is seen that on La^{3+} substitution, the saturation magnetization of Ni–Cu–Zn ferrites decreases. It may be attributed to the replacement of magnetic element (Fe^{3+}) by non-magnetic element (La^{3+}) on B-site, thereby decreasing B–B interaction and hence net magnetic moment reduces. Furthermore, non-magnetic La^{3+} ions substituted in the ferrite would weaken the interactions between magnetic particles and reduce resistance of the domain-wall motion, which caused the decrease in coercivity. Ren and Xu [37] reported similar type of result for La^{3+}-doped Ni–Co–Zn ferrites prepared by sol–gel method. They found that the addition of La^{3+} ions results in the decrease of saturation magnetization and coercivity. The effect of La^{3+} substitution on the structural and magneto-crystalline anisotropy of nano-crystalline cobalt ferrite synthesized by citrate precursor method was reported by Kumar and Kar [38]. They found that the saturation magnetization, magnetic coercivity, and magneto-crystalline anisotropy constants of ferrites were decreased with increase in La^{3+} concentration. From Table 4, it is observed that the Mr decreases with increase in La^{3+} content except $x=0.035$ composition. This is attributed to lowering the concentration of magnetic Fe^{3+} ions by non-magnetic La^{3+} ions. For the composition $x=0.035$, there may be possibility of increasing the concentration of Fe^{2+} ions during the synthesis process, and therefore, Mr is higher as compared to compositions $x=0.015$ and 0.025. It

Fig. 6 FE-SEM micro-photographs for $Ni_{0.7}Cu_{0.1}Zn_{0.1}La_xFe_{2-x}O_4$ (where $x=0.0$, 0.015, 0.025, and 0.035) system
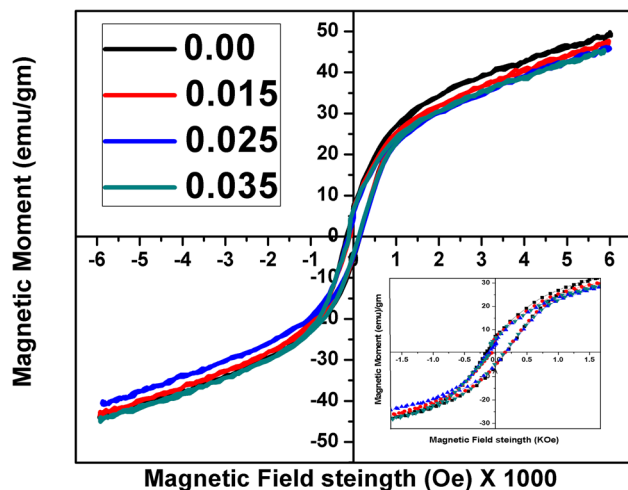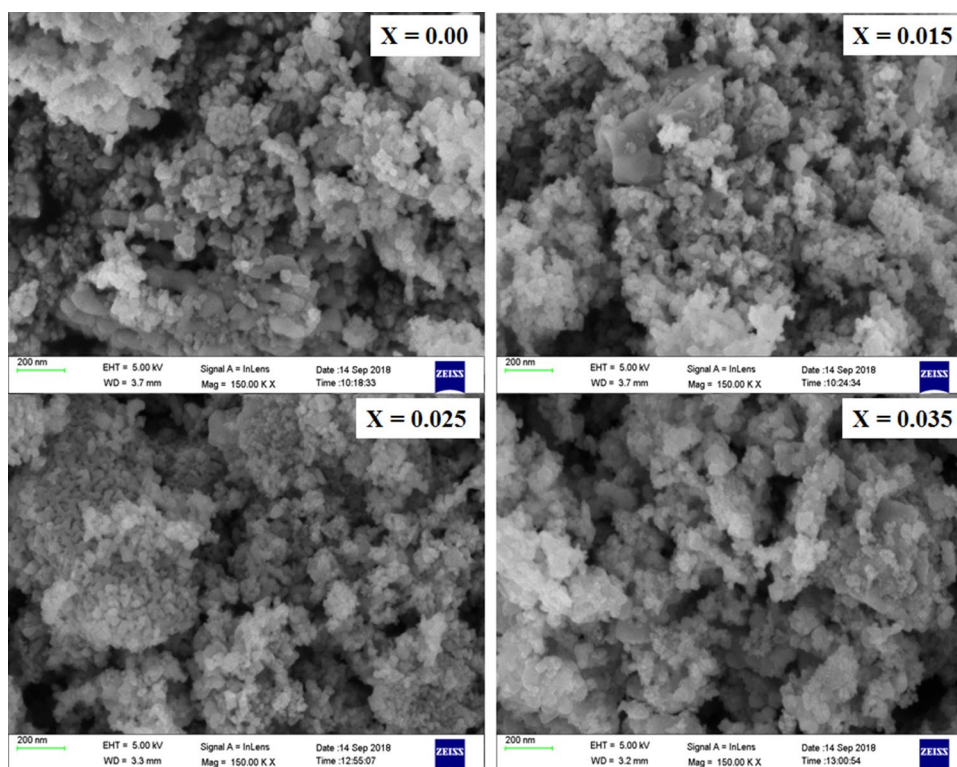
Fig. 7 Hysteresis loop for $Ni_{0.7}Cu_{0.1}Zn_{0.2}La_xFe_{2-x}O_4$ (where $x=0.0$, 0.015, 0.025, and 0.035) System

is also seen that Mr and H_c of La^{3+}-substituted Ni–Cu–Zn ferrites are lower than pure Ni–Cu–Zn ferrite [39, 40].

The squareness ratio (R), magnetic moment (η_B), and anisotropy constant (k_1) for all compositions were calculated using the relations [34]:

$$R = \frac{M_r}{M_S} \tag{10}$$

$$\eta_{B(Obs)} = \frac{MXM_S}{5585} \tag{11}$$

$$K_1 = \frac{H_C\,XM_S}{0.96}. \tag{12}$$

The values of R, $\eta_{B\,(obs)}$ and K_1 are listed in Table 4. From this table, it is cleared that η_B goes on decreasing with increase in La^{3+} content. This is may be due to the decreasing

Table 4 Magnetic parameters of $Ni_{0.7}Cu_{0.1}Zn_{0.2}La_xFe_{2-x}O_4$ (where $x=0.000$, 0.015, 0.025, and 0.035) system

Composition	Saturation magnetization M_s (emu/gm)	Remanence magnetization M_r (emu/gm)	Coercivity H_c (Oe)	Squareness ratio R	Magnetic moment $n_{B(obs)}$ μ_B	Anisotropy constant k_1 erg/cc
$Ni_{0.7}Cu_{0.1}Zn_{0.2}Fe_2O_4$	49.7877	6.88	157	0.1381	2.105614	8142.36
$Ni_{0.7}Cu_{0.1}Zn_{0.2}La_{0.015}Fe_{1.985}O_4$	47.6917	6.71	146	0.1407	2.027302	7253.11
$Ni_{0.7}Cu_{0.1}Zn_{0.2}La_{0.025}Fe_{1.975}O_4$	46.2013	6.05	155	0.1308	1.970818	7459.58
$Ni_{0.7}Cu_{0.1}Zn_{0.2}La_{0.035}Fe_{1.965}O_4$	45.4952	6.63	129	0.1456	1.947464	6113.41

saturation magnetization of ferrites with increasing La^{3+} content. Crystallographic, magnetic, and electrical properties of La^{3+}-substituted Ni–Cu–Zn nano-ferrites have been studied by Chaudhari et al. [19]. They reported that both observed and theoretical magnetic moments of Ni–Cu–Zn ferrites decrease with increasing La^{3+} content. Lenin et al. [41] synthesized La^{3+}-substituted nickel ferrite by sono-chemical reaction method. They reported that η_B of nickel ferrite found to be decreasing with increasing La^{3+} content.

Conclusion

La^{3+}-substituted Ni–Cu–Zn nano-ferrites were successfully synthesized by oxalate co-precipitation method at a low sintering temperature. EDAX shows the formation of appropriate stoichiometric ferrite under investigation. The formation of cubic spinel ferrite with weak ortho-ferrite phases due to $LaFeO_3$ was confirmed from XRD. The lattice constant of Ni–Cu–Zn ferrites increases with increase in La^{3+} content. The average crystallite size as well as grain size of all the ferrites are lies in nano-particle range and it verifies the formation of nano-ferrites. On La^{3+} substitution, grain size of the ferrites was decreased. The presence of absorption bands in the desired region of FTIR spectra confirms the formation of ferrites. Saturation magnetization and magnetic moment of ferrites decrease with increase in La^{3+} content. It is observed that the ferrite having composition $Ni_{0.7}Cu_{0.1}Zn_{0.2}La_{0.025}Fe_{1.975}O_4$ has smaller crystallite size, lower intensity, lower retentivity, and comparatively higher coercivity as compared to other La^{3+}-substituted compositions.

References

1. Hossain, S.S., Roy, P.K.: Structural and electro-magnetic properties of low temperature co-fired BaSrTiO₃ and NiCuZn ferrite composites for EMI filter applications. J. Mater. Sci. Mater. Electron. **28**, 18136–18144 (2017)

2. Nigel P. C., Schwaninger P., Widmer H.: Ferrite antennas for wireless power transfer. US Patent. **8**, 487–479 (2013)

3. Cogiore B., Kéradec J. P., and Barbaroux J.: The two winding ferrite core transformer: An experimental method to obtain a wide frequency range equivalent circuit.: In: Instrumentation and measurement technology conference, IMTC/93. Conference Record. IEEE, 558–562

4. Su, H., Zhang, H., Tang, X., Jia, L., Wen, Q.: Sintering characteristics and magnetic properties of NiCuZn ferrites for MLCI applications. Mater. Sci. Eng. B. **129**, 172–175 (2006)

5. Dantas, J., Leal, E., Mapossa, A.B., Cornejo, D.R., Costa, A.C.F.M.: Magnetic nanocatalysts of $Ni_{0.5}Zn_{0.5}Fe_2O_4$ doped with Cu and performance evaluation in transesterification reaction for biodiesel production. Fuel **191**, 463–471 (2017)

6. Lin, K., Adhikari, A.K., Tsai, Z., Chen, Y., Chien, T., Tsai, H.: Synthesis and characterization of nickel ferrite nano-catalysts for CO_2 decomposition. Catal. Today **174**, 88–96 (2011)

7. Jeseentharani, V., Reginamary, L., Jeyaraj, B., Dayalan, A., Nagaraja, K.S.: Nanocrystalline spinel $Ni_xCu_{08-x}Zn_{0.2}Fe_2O_4$: a novel material for humidity sensing. J. Mater. Sci. **47**, 3529–3534 (2012)

8. Gadkari, A.B., Shinde, T.J., Vasambekar, P.N.: Ferrite gas sensors. IEEE Sens. J. **11**, 849–861 (2011)

9. Kumbhar, V.S., Jagadale, A.D., Shinde, N.M., Lokhande, C.D.: Chemical synthesis of spinel cobalt ferrite ($CoFe_2O_4$) nano-flakes for supercapacitor application. Appl. Surf. Sci. **259**, 39–43 (2012)

10. Fu, Y., Wan, Y., Xia, H., Wang, X.: Nickel ferrite–graphene hetero architectures: Toward high-performance anode materials for lithium-ion batteries. J. Power Sources **213**, 338–342 (2012)

11. Shinde, B.L., Suryavanshi, V.S., Lohar, K.S.: Structural and magnetic properties of Cr^{3+} substituted nickel zinc copper nano ferrites. Int. J. Mater. Sci. **12**, 433–442 (2017)

12. Arulmurugan, R., Jeyadevan, B., Vaidyanathan, G., Sendhilnathan, S.: Effect of zinc substitution on Co–Zn and Mn–Zn ferrite nanoparticles prepared by co-precipitation. J. Magn. Magn. Mater. **288**, 470–477 (2005)

13. Assar, S.T., Abosheiasha, H.F., El Sayed, A.R.: Effect of γ-ray's irradiation on the structural, magnetic, and electrical properties of Mg–Cu–Zn and Ni–Cu–Zn ferrites. J. Magn. Magn. Mater. **421**, 355–367 (2017)

14. Sakar, M., Balakumar, S., Saravanan, P., Jaisankar, S.N.: Annealing temperature mediated physical properties of bismuth ferrite (BiFeO3) nanostructures synthesized by a novel wet chemical method. Mater. Res. Bull. **48**, 2878–2885 (2013)

15. Nejati, K., Zabihi, R.: Preparation and magnetic properties of nano size nickel ferrite particles using hydrothermal method. Chem. Central. J. **6**, 23 (2012)

16. Das, P.S., Singh, G.P.: Structural, magnetic and dielectric study of Cu substituted NiZn ferrite nanorod. J. Magn. Magn. Mater. **401**, 918–924 (2016)

17. Awati, V.V., Rathod, S.M., Shirsath, S.E., Mane, M.L.: Fabrication of Cu^{2+} substituted nanocrystalline Ni–Zn ferrite by solution combustion route: Investigations on structure, cation occupancy and magnetic behavior. J. Alloy. Compd. **553**, 157–162 (2013)

18. Shirsath, S.E., Kadam, R.H., Patange, S.M., Mane, M.L., Ghasemi, A., Morisako, A.: Enhanced magnetic properties of Dy^{3+} substituted Ni–Cu–Zn ferrite nanoparticles. Appl. Phy. Lett. **100**, 042407 (2012)

19. Chaudhari, V., Shirsath, S.E., Mane, M.L., Kadam, R.H., Shelke, S.B., Mane, D.R.: Crystallographic, magnetic and electrical properties of $Ni_{0.5}Cu_{0.25}Zn_{0.25}La_xFe_{2-x}O_4$ nanoparticles fabricated by sol–gel method. J. Alloy. Compd. **549**, 213–220 (2013)

20. Roy, P.K., Bera, J.: Enhancement of the magnetic properties of Ni–Cu–Zn ferrites with the substitution of a small fraction of lanthanum for iron. Mater. Res. Bull. **42**, 77–83 (2007)

21. Roy, P.K., Nayak, B.B., Bera, J.: Study on electro-magnetic properties of La Substituted Ni–Cu–Zn ferrite synthesized by auto-combustion method. J. Magn. Magn. Mater. **320**, 1128–1132 (2008)

22. Gabal, M.A., Asiri, A.M., AlAngari, Y.M.: On the structural and magnetic properties of La-substituted NiCuZn ferrites prepared using egg-white. Ceram. Int. **37**, 2625–2630 (2011)

23. Li, Y., Li, J., Li, Q., Yu, G., Zhang, H.: Structure and magnetic properties of NiCuZn ferrite materials with La doping. Rare Metals **36**, 202–204 (2017)

24. Mürbe, J., Töpfer, J.: High permeability Ni–Cu–Zn ferrites through additive-free low-temperature sintering of nanocrystalline powders. J. Eur. Ceram. Soc. **32**, 1091–1098 (2012)

25. Yue, Z., Li, L., Zhou, J., Zhang, H., Gui, Z.: Preparation and characterization of NiCuZn ferrite nanocrystalline powders by auto-combustion of nitrate–citrate gels. Mater. Sci. Eng. B **64**, 68–72 (1999)

26. Hsu, W., Chen, S.C., Kuo, P.C., Lie, C.T., Tsai, W.S.: Preparation of NiCuZn ferrite nanoparticles from chemical co-precipitation method and the magnetic properties after sintering. Mater. Sci. Eng. B. **111**, 142–149 (2004)

27. Ramakrishna, K.S., Srinivas, Ch., Meena, S.S., Tirupanyam, B.V., Bhatt, P., Yusuf, S.M., Prajapat, C.L., Potukuchi, D.M., Sastry, D.L.: Investigation of cation distribution and magnetocrystalline anisotropy of $Ni_xCu_{0.1}Zn_{0.9-x}Fe_2O_4$ nanoferrites: Role of constant mole percent of Cu^{2+} dopant in place of Zn^{2+}. Ceram. Int. **43**, 7984–7991 (2017)

28. Yan, S., Geng, J., Li, Y., Zhou, E.: Preparation of nanocrystalline NiZnCu ferrite particles by sol–gel method and their magnetic properties. J. Magn. Magn. Mater. **27**, 84–89 (2004)

29. Humbe, A.V., Kharat, P.B., Nawle, A.C., Jadhav, K.M.: Nanocrystalline Ni0.70$_{-x}$Cu$_x$Zn030Fe2O4 with $0 \leq x \leq 025$ prepared by nitrate-citrate route: structure, morphology and electrical investigations. J. Mater. Sci. Mater. Electron. **29**, 3467–3481 (2018)

30. Zhou, X., Jing, J., Liangchao, L., Feng, X.: Preparation and magnetic properties of La-substituted Zn–Cu–Cr ferrites via a rheological phase reaction method. J. Magn. Magn. Mater. **314**, 7–10 (2007)

31. Al-Angari, Y.M.: "Magnetic properties of La-substituted $NiFe_2O_4$ via egg-white precursor route. J. Magn. Magn. Mater. **323**, 1835–1839 (2011)

32. Shinde, T.J., Gadkari, A.B., Vasambekar, P.N.: Saturation magnetization and structural analysis of $Ni_{0.6}Zn_{0.4}Nd_yFe_{2-y}O_4$ by XRD, IR and SEM techniques. J. Mater. Sci. Mater. Electron. **21**, 120–124 (2010)

33. Augustin, C.O., Kalai, S.R., Nagaraj, R., Berchmans, L.J.: Effect of La^{3+} substitution on the structural, electrical and electrochemical properties of strontium ferrite by citrate combustion method. Mater. Chem. Phys. **89**, 406–411 (2005)

34. Kabbur, S.M., Ghodake, U.R., Nadargi, D.Y., Kambale Rahul, C., Suryavanshi, S.S.: Effect of Dy^{3+} substitution on structural and magnetic properties of nano-crystalline Ni–Cu–Zn ferrites. J. Magn. Magn. Mater. **451**, 665–675 (2018)

35. Waldron, R.D.: Infrared spectra of ferrites. Phys. Rev. **99**, 1727 (1955)

36. Ikram, S., Jacob, J., Arshad, M.I., Mahmood, K., Ali, A., Sabir, N., Amin, N., Hussain, S.: Tailoring the structural, magnetic and dielectric properties of Ni–Zn–$CdFe_2O_4$ spinel ferrites by the substitution of lanthanum ions. Ceram. Int. **45**, 3563–3569 (2019)

37. Ren, X., Guangliang, X.: Electromagnetic and microwave absorbing properties of NiCoZn-ferrites doped with La^{3+}. J. Magn. Magn. Mater. **354**, 44–48 (2014)

38. Kumar, L., Kar, M.: Effect of La^{3+} substitution on the structural and Magneto-crystalline anisotropy of nanocrystalline cobalt ferrite ($CoFe_{2-x}La_xO_4$)." Ceram. Int. **38**, 4771–4782 (2012)

39. Gholizadeh, A., Jafari, E.: Effects of sintering atmosphere and temperature on structural and magnetic properties of Ni–Cu–Zn ferrite nano-particles: magnetic enhancement by a reducing atmosphere. J. Magn. Magn. Mater. **422**, 328–336 (2017)

40. Ribeiro, U.L., Nasar, R.S., Nasar, M.C., Araújo, J.H.: Li quid phase sintering of ferrite of NiCuZn with low magnetic permeability for miniaturization. Ceram. Int. **44**, 723–727 (2018)

41. Lenin, N., Kanna, R.R., Sakthipandi, K., Kumar, A.S.: Structural, electrical and magnetic properties of NiLaxFe2-xO4 nanoferrites. Mater. Chem. Phys. **212**, 385–393 (2018)